JOURNAL OF MATERIALS SCIENCE 31 (1996) 6333–6338

Electron paramagnetic resonance spectra of CeO_2 catalyst for CO oxidation

C. OLIVA, G. TERMIGNONE, F. P. VATTI, L. FORNI
Dipartimento di Chimica Fisica ed Elettrochimica e Centro C.N.R. Universita' di Milano, Via Golgi 19 20133 Milano, Italy

A. V. VISHNIAKOV
D.I. Mendeleev University of Chemical Technology of Russia, Miusskaja Sq. 9, Moscow, Russia

The EPR spectra of freshly prepared CeO_2 samples as well as of samples used as a catalyst in the oxidation of CO to CO_2 are reported. Attribution of these patterns to oxygen species O_2^-, O_2, O^-, or to Ce^{3+} ions is discussed and dynamic phenomena involving these species are described. Bottlenecked systems between conduction electrons and Ce^{3+} ions are envoked to explain the observation of the Ce^{3+} EPR spectrum up to temperatures of about 370 K. Oxygen-deficient systems are obtained when the sample is used as a catalyst for CO oxidation in the presence of pyrex or quartz powder as a diluent, showing that the latter can play some role in stabilizing such species.

1. Introduction

CeO_2 possesses the ability to easily exchange oxygen with the atmosphere. Due to this property it has been frequently used as a catalyst or as a catalyst promoter in oxidation reactions.

In our laboratory CeO_2 is used, together with other transition metal oxides such as CuO, Fe_2O_3, CoO, to form catalysts for CO oxidation. Before detailed examination of these catalysts can be performed it is important to gain a detailed understanding of the characteristics of CeO_2, in particular its paramagnetic properties and its interaction with adsorbed oxygen. In the present work we report electron paramagnetic resonance (EPR) spectra measured on both freshly prepared CeO_2 and with samples of the same batch after use as a catalyst in CO oxidation with air. The catalytic behaviour of cerium oxide will be reported in detail elsewhere, in comparison with other mixed transition metal oxide catalysts.

Paramagnetic oxygen species adsorbed on CeO_2 have been reported in the literature [1–4]. The line with $g_{zz} \cong 2.03$ has been attributed to O_2^- adsorbed on either CeO_2, [2] or on CeO_2–SiO_2, [3] or on Ce/Al_2O_3 and Ce–Pd/Al_2O_3 [4]. The small difference between the values reported for g can be due to a small difference in the oxidation state of the sample, entailing significant changes in the value of g_{zz} of O_2^- [3]. Furthermore, a value of $g_\perp = 2.014$ has been attributed to O_2^- adsorbed on CeO_2 [2]. The same parameter was evaluated to equal 2.011 for Ce/Al_2O_3 and Ce–Pd/Al_2O_3 [4]. Values of $g_x = 2.016$ and $g_y = 2.01$ were found with CeO_2–SiO_2 [3] which were attributed to O_2^-. In none of these references is an EPR line attributed to O^- ions. A recent Fourier transform-infrared (FT-IR) spectroscopy investigation suggested that adsorbed O_2^- species are generally favoured over O^- species on cerium oxide [5]. In the same paper it was shown that the adsorption of O_2 on well-degassed CeO_2 (1000 K) leads to the formation of O_2^- and O_2^{2-} surface species, and that only the former species can exchange site via gaseous O_2 molecules. However, O_2^{2-} is not paramagnetic. Therefore, the oxygen-based species that can be detected in EPR spectra with CeO_2 are only O_2^- and O_2. It should be noted that an extra more intense EPR line with $g = 1.964$ is generally found in these patterns. This line has been attributed either to quasi free electrons for oxygen adsorbed on CeO_2 [2] as well as on ZnO [6–9], or to Ce^{3+} in the case of a partially reduced CeO_2/SiO_2 catalyst at 77 K [3].

Ce^{3+} is a paramagnetic ion, which is described as a system with one unpaired electron in the 4f state. The theory of its paramagnetism is well established and has been widely reviewed [10–16]. However, very few experimental evaluations [15–17] of the corresponding EPR patterns are reported in the literature. Indeed, the Ce^{3+} EPR signal is thought to be unmeasurable at high temperature, due to dipolar effects and exchange interactions [2]. A "magnetic dilution" is needed to overcome such effects, but even in this case the signal can be detected only below 20 K, due to fast spin-lattice relaxation.

2. Experimental procedure

CeO_2 samples were obtained by the calcination of Ce^{3+} nitrate (Janssen, hexahydrate, $\geqslant 99.5\%$ pure, used as purchased) in slowly flowing air at 950 °C for 3 h. The EPR spectra were recorded by means of a Bruker ESP 300 EPR-ENDOR instrument,

0022–2461

equipped with an ER4111-VT thermostatic device and with an Oxford Instruments liquid helium cryostat. The magnetic field ranged from 0–0.5 T, and the spectra were collected at temperatures between 10–623 K.

Temperature-programmed desorption (TPD) spectra were collected from the CeO_2 samples that were held in a 20 $cm^3 min^{-1}$ flow of extrapure He ($\geq$ 99.9999 vol %). The initial temperature dwell was 30 °C for 30 min, followed by the TPD ramp (20 °C min^{-1}) up to a final dwell at 550 °C, held for 30 min. The detector was a UTI Model 100 C QMS.

CeO_2, either pure or mixed with powdered pyrex glass, was used as a catalyst for CO oxidation. The latter was carried out in a continuous fixed-bed microreactor, by feeding a CO + N_2 mixture (1 vol % CO) and air (50 vol % each) at a 40 $cm^3 min^{-1}$ overall gas flow rate. The reaction temperature was 250 °C.

3. Results

3.1. EPR spectra of "fresh" CeO_2

EPR spectra were collected with fresh (i.e., not used as a catalyst) CeO_2 and are shown in Fig. 1. They show six α to ζ lines in the 0.32–0.35 T region, characterized by the nearly temperature independent g values; 2.046, 2.034, 2.021, 2.009, 1.964 and 1.947 respectively. The intensity of all these lines decreased at higher temperatures, as is clear from Fig. 1. A decrease in the intensity was also noticed at every temperature after a TPD run. After the latter the EPR patterns (see Fig. 2) were rather temperature-independent, with the sole exception of the δ (g = 2.009) line, which continuously narrowed up to room temperature and then became temperature-independent as with the other lines.

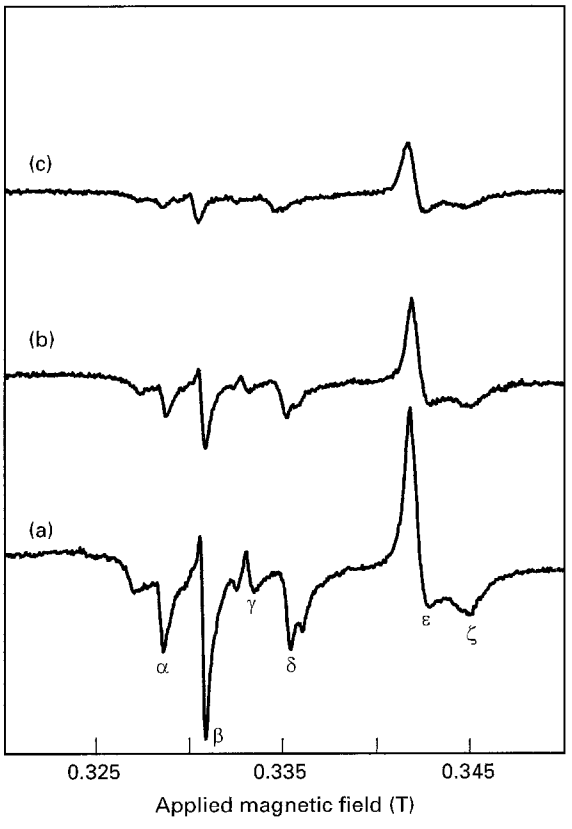

Figure 1 EPR patterns of fresh CeO_2 in the 0.32–0.35 T range at (a) 130, (b) 270 and (c) 370 K.

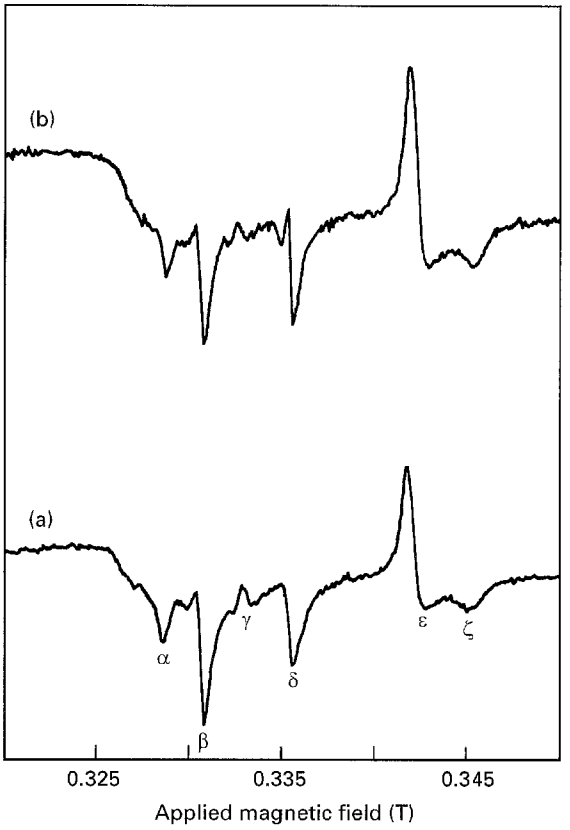

Figure 2 EPR patterns of fresh CeO_2 after the TPD run of Fig. 7. Spectra recorded at (a) 153, (b) 293 K.

3.2. EPR spectra of CeO_2 after use as catalyst

The spectral patterns were less intense than before the catalytic reaction. Furthermore, after a TPD run just the ε and ζ lines (see Fig. 3) were nearly temperature-independent, whilst at higher temperatures all the other lines became less intense. In particular, the δ line was dramatically temperature-broadened, which is opposite behaviour to that displayed by that line in the case of a fresh sample after TPD, when it became temperature-narrowed (compare Fig. 3 with Fig. 2).

3.3. EPR patterns at low temperature

At low temperature (10 K) the fresh sample displayed a completely new EPR spectrum (Fig. 4). The lines with g values between 2.046 and 2.009 irreversibly disappeared. We were not able to regenerate these lines even after annealing up to room temperature. On the other hand, the ε and ζ lines were still observable. In addition a new line at $g \cong 4$ was observed. The whole EPR pattern of a sample used in the CO oxidation underwent an intensity decrease.

3.4. EPR spectra in the presence of pyrex or quartz powder

Generally CeO_2, before use as catalyst, was diluted (1:1 by weight) with pyrex glass powder to reduce the

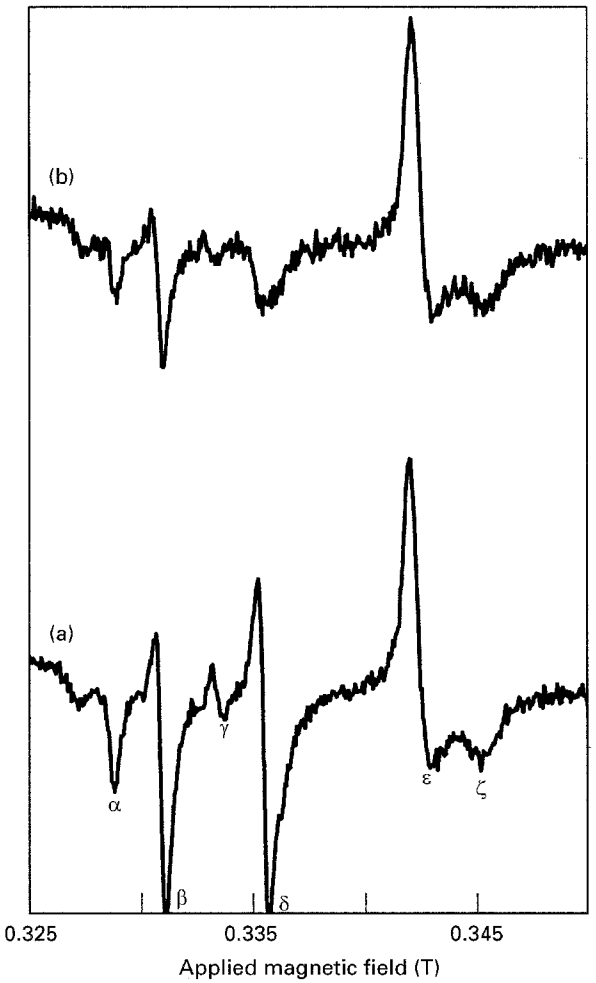

Figure 3 EPR pattern of CeO_2 (diluted in pyrex powder) after use as a catalyst for the oxidation of CO at 250 °C and after the TPD run of Fig. 8. EPR recording temperature: (a) 130, (b) 270 K. α: $g = 2.046$; β: $g \cong 2.034$; γ: $g = 2.021$; δ: $g = 2.009$; ε: $g = 1.964$; ζ: $g = 1.947$.

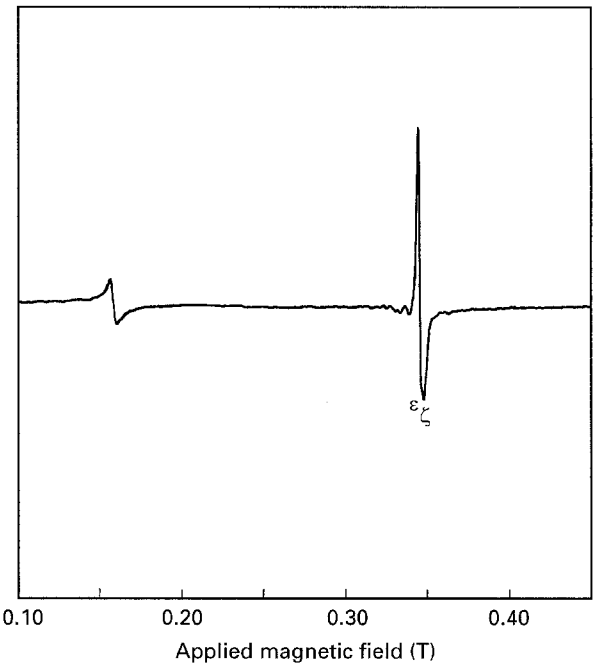

Figure 4 EPR pattern of fresh CeO_2 at 10 K.

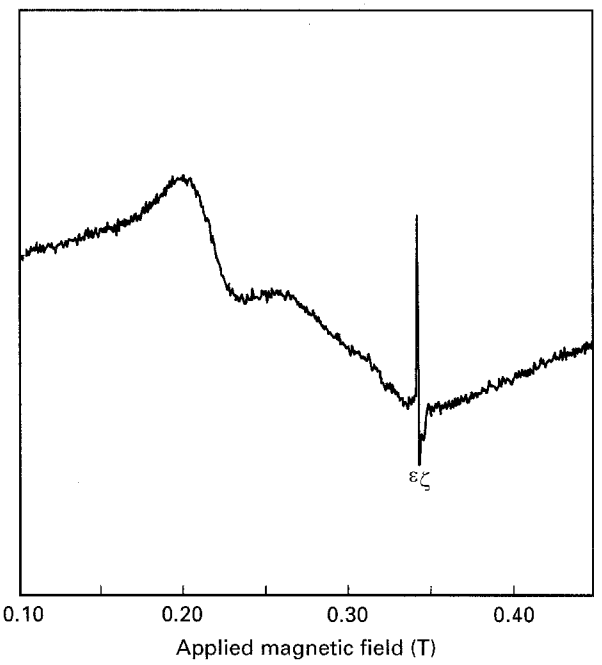

Figure 5 Room temperature EPR pattern of CeO_2 sample mixed with quartz powder and used as a catalyst for the oxidation of CO with O_2. Fresh sample chilled to 10 K.

risk of hot spots. Samples of this kind have also been examined by EPR. The presence of pyrex did not significantly influence the α to ζ EPR lines. On the contrary, in the pyrex containing samples other EPR lines were occasionally found in the low field region, probably due to chemical impurities in the glass. In order to eliminate such impurities, the experiment was repeated using quartz powder. At room temperature, after use as catalyst, the sample spectrum no longer contained the EPR line with $g \cong 4$, whilst a nearly 0.03 T broad band at about 0.21 T was observed. This can be seen in Fig. 5 for a sample previously cooled to 10 K. Similar patterns were also obtained, after the CO oxidation reaction, using pyrex instead of quartz powder and also in samples not previously cooled. The only difference, in the last case, was the additional presence of the previously discussed α, β, γ, and δ EPR lines. In all these cases the band at 0.21 T moved to higher field values (Fig. 6) after a TPD run.

3.5. TPD of fresh CeO_2

The fresh CeO_2 sample was observed to adsorb oxygen up to about 240 °C, and then to release it during the TPD ramp and final dwell (Fig. 7), suggesting that the oxide has not become any more oxygen deficient. After the TPD experiment, the EPR spectra shown in Fig. 2 were recorded.

3.6. TPD of CeO_2 after use as catalyst for CO oxidation at 250 °C

The TPD spectrum measured on CeO_2 after use in the oxidation of CO at 250 °C is reported in Fig. 8. One may observe that this sample adsorbs oxygen up to about 550 °C and continues the adsorption during the

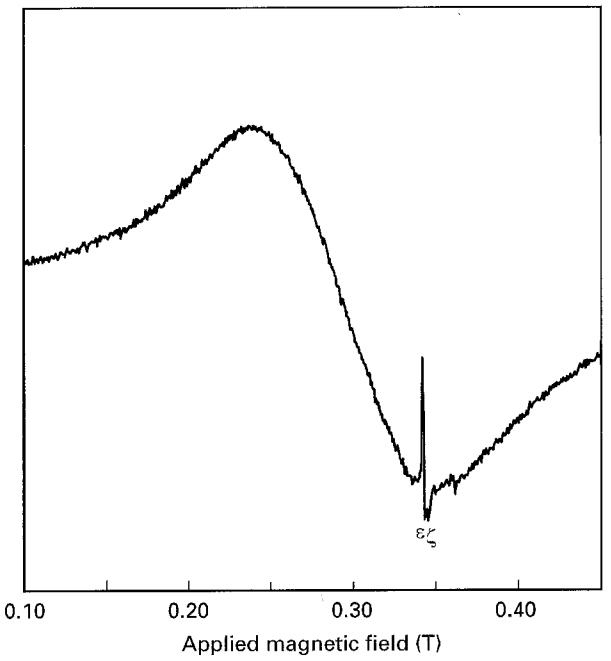

Figure 6 EPR pattern of the same sample of Fig. 5, after a TPD run.

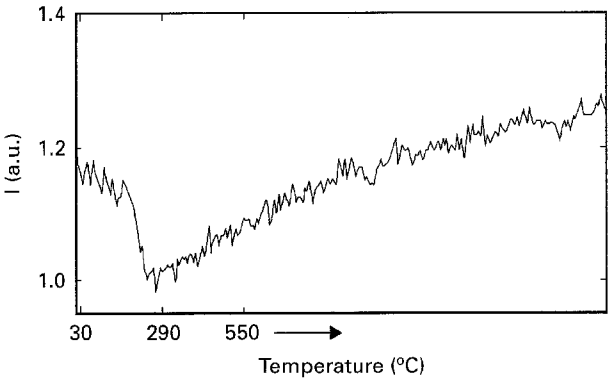

Figure 7 TPD spectrum of oxygen (a.m.u. = 32) on fresh CeO_2.

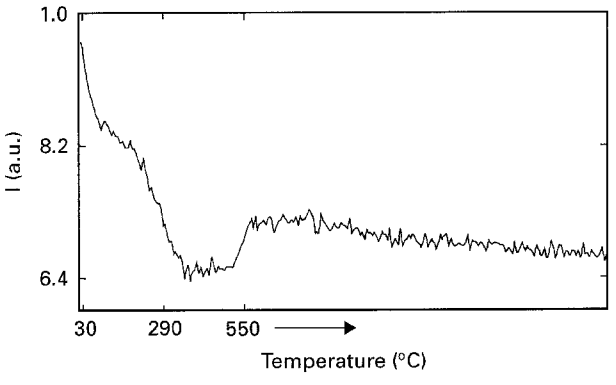

Figure 8 TPD spectrum of oxygen (a.m.u. = 32) on CeO_2 after CO oxidation at 250 °C.

final isothermal dwell at this temperature. This suggests that the sample is still oxygen deficient after the TPD experiment, although the amount of adsorbed oxygen is 1.7 times the amount adsorbed by the fresh sample during the analogous TPD experiment (compare with Fig. 7).

4. Discussion

4.1. Attribution of the EPR lines α, β, γ, and δ

All the EPR lines α to δ (observed in the g range between 2.046 and 2.009) can be attributed to physisorbed oxygen molecules or to paramagnetic species such as O_2^- generated from these oxygen molecules. In fact it has been observed [18, 19] that the magnitude of g_{zz} for O_2^- depends on the nature of the adsorption site. Indeed in the equation:

$$g_{zz} = g_e + \frac{2\lambda}{\Delta} \quad (1)$$

the parameter Δ is sensitive to the crystal-field gradient across the O_2^- ion, and in particular to the oxidation state of the nearest cation. We are led then, to attribute all these lines to O_2^- species in different environments, as proposed by Zhang and Klabunde [20] with a similar but differently prepared sample. In that paper this attribution was justified by many experimental observations. However, in the present case some experimental findings suggest a slightly different conclusion.

Furthermore, some of our results are similar to those reported in other papers. For instance, lines with $g = 2.045$ have been reported with ZnO [9, 21] and MgO [22] and attributed to O^-. However this attribution is still controversial, and significantly it is dependent on the chemical nature of the substrate. For example, a line with $g = 2.04$ has been attributed [7] to O_2 adsorbed on ZnO, O_2^- in that case being considered EPR-silent, whilst the values $g_{zz} = 2.043$, $g_{xx} = 2.002$ and $g_{yy} = 2.008$ were attributed [23] to O_2^- ions adsorbed on La_2O_3/CaO. As previously mentioned, O^- cannot easily adsorb on to CeO_2, whilst the line with $g = 2.045$ is rather intense. Therefore we could tentatively attribute the EPR line with $g = 2.045$ to the adsorbed O_2 as in reference [7] or to O_2^- located in surface oxygen vacancies as in reference [20]. However, the latter attribution seems the most correct in the present case, while other considerations would lead us to attribute the EPR line with $g = 2.009$ to adsorbed O_2, in contrast with reference [20]. In fact, in the case of Fig. 3 in which the sample is still oxygen deficient (as shown by the TPD run of Fig. 8) all the EPR spectra with $2.0046 < g < 2.009$ broaden at higher temperature when further amounts of O_2 adsorb, but this broadening is particularly noticeable for the δ line ($g = 2.009$). As a consequence this line can be confidently attributed to adsorbed O_2 molecules, that are the species which more easily exchange with other gaseous O_2 molecules in the surrounding atmosphere. We note that this broadening is only observed when the recording temperature is kept high enough. It is not observed when the EPR spectrum is recorded at room temperature, immediately after heating the sample. Thus the broadening must be attributed to a dynamic temperature-dependent phenomenon. Furthermore, this broadening is not observed in cases similar to that reported in Fig. 2, in which the sample is not oxygen deficient (as shown by the TPD run of Fig. 7, carried out before recording

the EPR spectrum of Fig. 2). On the contrary, in this case the δ line narrows at higher temperature, suggesting that the adsorbed O_2 molecules rapidly diffuse amongst different surface sites.

4.2. Attribution of the EPR lines ε and ζ

The ε EPR line ($g = 1.964$) has been attributed both to quasi free electrons [2, 3, 6–9] and to Ce^{3+} ions [23]. The former attribution would be supported by the fact that Ce^{3+} has a short spin-lattice relaxation time, and therefore it could be difficult for it to display such a narrow line even at temperatures higher-than-room temperature. However, the shape of this line, as well as the shape of the nearest neighbour line ζ at $g = 1.947$, would suggest that they are both produced by the same paramagnetic species, namely by cerous ions with a distorted symmetry. To explain the unexpected observation of the Ce^{3+} spectrum even at high temperature, we propose that both e^- and Ce^{3+} can contribute to this EPR pattern forming a bottlenecked system. In fact, the presence of the mobile conduction electron (CE) requires that the interaction of its spin σ with the spin S of the Ce^{3+} ions, as well as with the spins of the other ions such as O_2^-, must be taken into account. The scattering between CE and Ce^{3+} ions would produce a new spin-flip relaxation process characterized by a rate δ_{ie} (Korringa-rate, increasing with temperature) and by its inverse δ_{ei} (Overhouser-rate, increasing with the concentration of Ce^{3+}). At very low Ce^{3+} concentrations, the exchange rate δ_{ei} would be negligible and the temperature-dependent EPR line-width of the Ce^{3+} EPR spectrum (ΔH) would be given by:

$$\Delta H = a + bT \tag{2}$$

where a and b are constants. This "normal" situation is called isothermal. The presence of the line-broadening contribution of Equation 2 makes the Ce^{3+} EPR spectrum generally undetectable at $T > 20$ K.

At higher Ce^{3+} concentrations, however, the CE and the local moments of Ce^{3+} ions can form a dynamic strongly coupled resonance system (the so-called bottleneck). The degree of the bottleneck is conveniently defined as:

$$d = \frac{\delta_{eL}}{\delta_{ei} + \delta_{eL}} \tag{3}$$

where $d = 1$ for the isothermal limit ($\delta_{ei} = 0$), $d = 0$ for the extreme bottleneck limit ($\delta_{eL} = 0$). Both δ_{eL} and δ_{ei} depend on the value of the concentration c_i of the Ce^{3+} ions. This fact results [24, 25] in a more bottlenecked system at higher c_i values, at least up to some critical value c_i'. For $c_i > c_i'$, then, d can become independent of c_i. In the bottlenecked case, both the g shift and the EPR line-width of the Ce^{3+} ions can be expressed by:

$$\Delta g = d^2 \Delta g_{iso} \tag{4}$$

$$\Delta H = d \Delta H_{iso} \tag{5}$$

Equation 5 shows that in a bottlenecked system the EPR lines narrow becoming detectable though they were not where in the isothermal condition. Furthermore, the line-width temperature dependence, in the isothermal case given by Equation 2, is attenuated in the bottlenecked case as the system approaches the extreme bottlenecked situation, that is for $d \to 0$.

This can also explain the fact that the intensity of the ε and ζ lines shows only a small change with temperature down to at least 10 K (Fig. 4). At low temperature the ε and ζ lines have nearly the same intensity as at room temperature, while all the α to δ lines, attributed to gaseous O_2 or O_2^- molecules, disappear as the oxygen liquifies. The new pattern observed at 0.15 T (Fig. 4) can thus be attributed to liquid oxygen in the triplet state rather.

We still have to explain why at higher temperatures the intensity of the ε and ζ lines decreases in the fresh sample (Fig. 1) but do not decrease after a TPD run using that same sample (Fig. 2), nor with the used sample after a TPD run (Fig. 3). In our opinion this can be explained by considering that in both these cases, after the TPD run, more oxygen adsorption has occurred on the sample, which favours the decomposition of the O_2^- ions present on the surface via the reaction:

$$O_{2\,ads}^- \rightarrow e^- + O_{2\,ads} \tag{6}$$

This would increase the concentration of e^- forming bottlenecked systems with Ce^{3+}, and eventually an extreme bottlenecked limit could be reached, in which a temperature-independent Ce^{3+} EPR line-width is detected.

The g values of 1.964 and 1.947, attributed to Ce^{3+} ions, are slightly different from the values found in the literature for this ion. In fact, a theoretical value [15] of $g = -1.4286$ has been calculated for Ce^{3+} ions embedded in a crystal of cubic symmetry, while experimental values of $g = 1.3085$ (in SrS powder at 20 K [15]), and $g = 1.37$ (in LaP at $T < 5$ K [16]) have been reported which are in good agreement with the theoretical value. However, also in the cubic system, some deviations from the theoretical g-value were noticed [15, 16]. The most striking effect is reported [16] in the case of LaP doped with Ce, when the sample was cooled under a magnetic field of 0.5 T. In this case an angular independent value $g = 2.93$ was measured, which is considerably different to the value reported above for the experiment performed under normal conditions. The formation of a ferrimagnetic phase during the field-cooling process is thought to explain this unexpected result. In fact a value of $g^* = 2.57$ can be calculated in this case using the Wangsness formula [17], when combining ferromagnetically one-Γ_7 sublattice with two-Γ_8 sublattices. This kind of structure would be supported by neutron diffraction measurements, performed below 4 K [16], although this produces a value of $g^* = 4.85$. In any case, the formation of ferrimagnetic state via $\Gamma_7 - \Gamma_8$ mixing would be able to explain such high g values even in the case of cubic structures. Therefore, a deviation of the g factor from its theoretical value can be explained, as in the present case, through many mechanisms.

4.3. Attribution of the EPR lines at 2100 G

The combination of paramagnetic sublattices could also account, by application of the Wangsness theory [17], for the broad EPR band observed at about 0.21 T after reaction with CO (Fig. 5). A statistical model for partially ordered defects obtained with hypostoichiometric metal oxides such as CeO_{2-x} is available in literature [26]. However, we must note that this EPR band was observed only in samples mixed with pyrex or quartz powder, which therefore must play an essential role in its formation. Furthermore, no other line attributable to any oxygen species is observed in the spectrum of Fig. 5. In fact, at room temperature the line at 0.15 T, assigned to oxygen in a triplet state, disappeared, and in the case of the previously cooled sample (Fig. 5) the α to δ lines also vanished. Though a contribution of cerium subdomains to the band at 0.21 T can be invoked, oxygen species must also be involved in its formation, through the support given to them by the pyrex or quartz powder particles present in the sample. This is further confirmed by the fact that after the TPD run of Fig. 8, i.e., after a further oxygen adsorption onto the sample, the band changes, moving towards lower g values (see Fig. 6). We can thus conclude that the band at 0.21 T is associated with the presence of oxygen adsorbed onto the glass particles which probably also interact with Ce^{3+} ions but in a situation of oxygen deficiency, while the EPR line of Fig. 6 corresponds to the situation in which there is no more oxygen deficiency. Furthermore, we must note that the broad bands of Figs 5 and 6 were not observed in samples of pure pyrex particles that had been heated up to 250 °C for 5 h in air, nor with samples of pyrex treated with CO. Only the simultaneous presence of glass, CeO_2 and CO leads to these spectra.

5. Conclusions

CeO_2 is an oxygen-deficient system which easily adsorbs O_2 from its surroundings and exchanges the adsorbed molecules with gaseous ones. EPR spectra attributable to O_2 and O_2^- species are observed with this sample, with dynamic equilibria existing between all these paramagnetic systems. Furthermore, bottlenecked and even extreme bottlenecked situations are obtained through the interaction of Ce and Ce^{3+} ions. This can explain the unexpected observation of an EPR spectra for Ce^{3+} existing at a temperature as high as 370 K.

References

1. M. SETAKA and T. KWAN, *Bull. Chem. Soc. Jpn.* **43** (1970) 2727.
2. M. GIDEONI and M. STEINBERG, *J. Solid State Chem.* **4** (1972) 370.
3. M. CHE, J. F. J. KIBBLEWHITE and A. J. TENCH, *J.C.S. Faraday Trans.* **69** (1973) 857.
4. A. S. SASS, V. A. SHVETS, G. A. SAVEL'EVA, N. M. POPOVA and V. B. KAZANSKII, *Kinetika i Kataliz* **26** (1985) 924.
5. C. LI, K. DOMEN, K. -I. MARUYA and T. ONISHI, *J. of Catal.* **123** (1990) 436.
6. R. J. KOKES, *J. Phys. Chem.* **66** (1962) 99.
7. K. M. SANCIER, *J. of Catal.* **5** (1966) 314.
8. M. CODELL, H. GISSER, J. WEISBERG and R. D. IYENGAR, *J. Phys. Chem.* **72** (1968) 2460.
9. J. O. COPE and I. D. CAMPBELL, *J.C.S. Faraday Trans.* **69** (1973) 1.
10. A. ABRAGAM and B. BLEANEY, "Electron paramagnetic resonance of transition ions" (Dover Publications, New York, 1986) pp. 308–12.
11. *Idem, ibid.* Ch. 18.
12. D. M. S. BAGGULEY and G. VELLA-COLEIRO, *J. Phys. C (Solid St. Phys.)* **2** (1969) 2310.
13. R. J. BIRGENEAU, *Phys. Rev. Lett.* **19** (1967) 160.
14. B. R. JUDD, *Proc. R. Soc.* **A 232** (1955) 458.
15. J. KREISSL, *Phys. Stat. Sol. (b)* **180** (1993) 441.
16. K. KINDO, T. SHIBATA, T. INOUE, Y. HAGA, T. SUZUKI, Y. CHIBA and M. DATE, *J. Phys. Soc. Jpn.* **62** (1993) 4190.
17. R. K. WANGSNESS, *Phys. Rev.* **91** (1953) 1085.
18. C. LOUIS, T. L. CHANG, M. KERMAREC, T. LE VAN, J. M. TATIBOUET and M. CHE, *Colloids and Surfaces A: Physicochem. and Engineering Aspects* **72** (1993) 217.
19. R. F. HOWE, *ibid.* **72** (1993) 353.
20. X. ZHANG and K. J. KLABUNDE, *Inorg. Chem.* **31** (1992) 1706.
21. N.-B. WONG, Y. B. TAARIT and J. H. LUNSFORD, *J. Chem. Phys.* **60** (1974) 2148.
22. E. GIAMELLO, L. CALOSSO, B. FUBINI and F. GEOBALDO, *J. Phys. Chem.* **97** (1993) 5735.
23. T. YANG, L. FENG and S. SHEN, *J. of Catal.* **145** (1994) 384.
24. K. BABERSCHKE, *Z. Physik* **B 24** (1976) 53.
25. M. ZOMACK, K. BABERSCHKE and S. E. BARNES, *Phys. Rev. B* **27** (1983) 4135.
26. L. M. ATLAS, *J. Phys. Chem. Solids* **29** (1968) 91.

Received 2 February 1995
and accepted 8 May 1996